Underlayer material influence on electric-field controlled perpendicular magnetic anisotropy in CoFeB/MgO magnetic tunnel junctions

Witold Skowroński,[1,2,*] Takayuki Nozaki,[1] Duong D. Lam,[1] Yoichi Shiota,[1] Kay Yakushiji,[1] Hitoshi Kubota,[1] Akio Fukushima,[1] Shinji Yuasa,[1] and Yoshishige Suzuki[1,3]

[1]*National Institute of Advanced Industrial Science and Technology, Spintronics Research Center, Tsukuba, Ibaraki 305-8568, Japan*

[2]*AGH University of Science and Technology, Department of Electronics, Al. Mickiewicza 30, 30-059 Kraków, Poland*

[3]*Graduate School of Engineering Science, Osaka University, Osaka 560-8531, Japan*

(Received 9 March 2015; published 18 May 2015)

We study the dependence of the perpendicular magnetic anisotropy on the underlayer material in magnetic tunnel junction. Using several different 4d and 5d metals we identify an optimal seed layer in terms of high anisotropy, low mixing, and high thermal stability. In such systems we investigate the tunability of the anisotropy by means of electric fields. Especially, by using W as the underlayer of the CoFeB/MgO/CoFeB trilayer we could obtain good thermal stability that allows for annealing in the temperatures up to 450 °C, which results in high perpendicular anisotropy.

DOI: 10.1103/PhysRevB.91.184410 PACS number(s): 85.75.Dd, 75.30.Gw, 76.50.+g, 73.61.At

I. INTRODUCTION

Magnetic multilayer systems with perpendicular magnetic anisotropy have been at the center of extensive studies in the past couple of decades, because of their application possibilities in both capacious disk drive media and magnetic random access memories (MRAM) [1]. In recent years, the ability to manipulate the magnetic anisotropy in metallic systems by means of the electric field has been discovered [2,3], which led to a proof-of-concept presentation of MRAM unit cell [4–6], spin torque oscillator [7], magnetic field sensor [8], and a control of domain wall motion [9,10] in multilayer thin films. In all these systems, the perpendicular magnetic anisotropy (PMA) of the ferromagnet/insulator interface was used and controlled by applying voltage across the insulator. However, for practical application, the change of the PMA with the electric field should be increased to around 1 pJ/Vm.[1]

One possibility of enhancing the voltage controlled magnetic anisotropy (VCMA) is to combine different underlayer and/or capping materials [11]. It was suggested in Ref. [12] that the magnitude of the VCMA is correlated with the efficiency of the Rashba effect at the interfaces, and thus, with spin-orbit coupling. Moreover, it was proposed that the sign of VCMA can be inverted by changing the neighboring material from 4d to 5d metal, which was indeed measured [13]. Therefore, it is of great importance to verify different heavy metal/ferromagnet/insulator systems in order to maximize the VCMA. In this work, we present a systematic experimental study on underlayer material influence on PMA. We explore the annealing temperature effect on magnetic properties. Finally, on selected samples we investigate VCMA in a static and dynamic regime.

II. EXPERIMENT

We sputter-deposited the following multilayer system (thickness in nm): Ta (5)/M (5)/$(Co_{15}Fe_{85})_{80}B_{20}$ (0.88)/MgO (2.5)/$(Co_{15}Fe_{85})_{80}B_{20}$ (0.6 or 5)/Ta (5)/Ru (5)/Pt (2), on chemical-mechanical-polished Si substrate, with (stack A) 0.6-nm and (stack B) 5-nm thick top CoFeB for magnetic and transport measurements, respectively. The underlayer material M was changed between Ir, CuN, Ag, Zr, Nb, W, Pd, and Pt. After the deposition process, the samples with stack A were successfully measured using the vibrating sample magnetometer (VSM) and annealed in a high-vacuum furnace at temperatures ranging from 170 °C up to 450 °C. This thickness of top CoFeB ensures lack of magnetization due to a mixing with Ta; consequently all magnetic signal is ascribed to the bottom CoFeB layer. At the same time, the structure maintains similar materials order as stack B for transport measurements (with in-plane magnetized thick CoFeB), which were patterned into rectangle-shape devices with the dimensions of 2 and 6 μm, using optical lithography, ion-beam milling, and lift-off processes. Afterwards, the selected devices were measured at room temperature in a high-frequency probe station with the sample stage rotating in two axes, with the magnetic field applied up to 2 T. The MgO thickness of $t_{MgO} = 2.5$ nm resulted in a resistance area product of about 100 kOhm × μm^2, which limits the current density to values below 1kA/cm^2. Static properties were measured using a direct-current source meter with the ground electrode connected always to the buffer of the MTJ. In order to verify repeatability and potential high operation speed of designed MTJ, radio-frequency (RF) rectification measurements were also performed [14]. To do so, an amplitude modulated RF signal of power $P = 0$ dBm was fed to the MTJ via high-frequency bias T and the magnetic field applied at an angle between parallel and perpendicular to the sample plane was swept and the mixing signal V_{mix} was measured using the lock-in amplifier. Due to the impedance mismatch between our 50-Ohm measurement setup and the MTJ samples with the resistance of a few kOhm, the actual power delivered to the MTJ is about P = 20 μW. The resulting FMR spectra were analyzed using the model presented elsewhere [15].

*skowron@agh.edu.pl

[1]For the magnetic memory bit of 10–30 nm in diameter, the product of K_{eff} and t should be of the order of $K_{eff} \times t = 1$–3 mJ/m^2, in order to keep sufficient thermal stability. Corresponding surface energy of an electric field of 1 V/nm, requires the slope of the VCMA effect of more than 1 pJ/Vm.

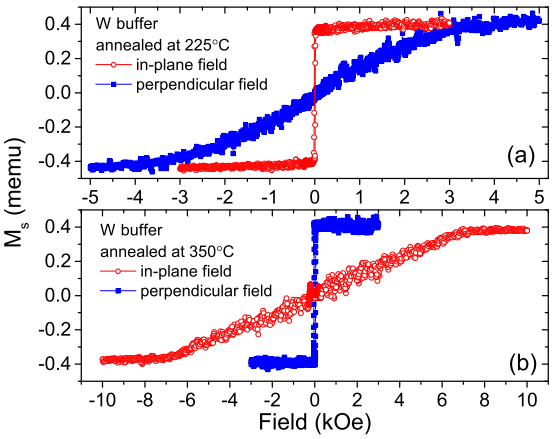

FIG. 1. (Color online) VSM measurements of the sample on the W buffer annealed at (a) 225 °C and at (b) 350 °C in both in-plane and perpendicular fields.

III. RESULTS AND DISCUSSION

A. PMA dependence on underlayer

The most relevant parameters for systems exhibiting PMA are the saturation magnetization and the effective anisotropy K_{eff} of the bottom CoFeB layer, both of which can be determined from the VSM measurements. K_{eff} is defined as

$$K_{\text{eff}} = K_{\text{i}}/t + K_{\text{V}}, \tag{1}$$

where K_{i} is an interface anisotropy, t is the bottom CoFeB layer thickness, and K_{V} is the volume anisotropy, which we attribute to the demagnetizing field $K_{\text{V}} = -\mu_0 M_{\text{s}}^2/2$. However, both of these quantities are also affected by the magnetic dead layer, which requires precise analysis of ferromagnet thickness dependence of aforementioned parameters. Therefore, instead we plot M_{s}/A, with M_{s} and A being the magnetic moment and area of measured samples, respectively, and the saturation field H_{s} as a function of annealing temperature, as these give us information about relevant material systems with PMA [16]. An example of the VSM measurement results for the W buffer annealed at 225 °C and 350 °C is presented in Fig. 1.

Figure 2(a) presents the M_{s}/A for investigated MTJ with different underlayer material as a function of annealing temperature. An increase in M_{s}/A is noted in all underlayer cases upon first annealing at 170 °C, which can be explained by a slight B diffusion into MgO and/or underlayer [17]. In the next annealing steps for most of the materials (except from W and Nb), the M_{s}/A starts to degrade, which is a signature of a mixing between CoFeB and the underlayer metal. In both the W and Nb cases (and especially for the Zr buffer) the initial M_{s}/A after the deposition is smaller than for other samples that can be explained by an interlayer formation that reduces M_{s} or the effective CoFeB thickness, but prevents bilayer from further mixing. In our case, using Pd or Pt buffers did not result in transition to PMA in the CoFeB layer even after the thermal treatment.

Next, we comment on the PMA change after annealing. H_{s} varies significantly between samples with different underlayers and changes from negative (in-plane effective anisotropy) to positive values (effective PMA); see the results in Fig. 2(b).

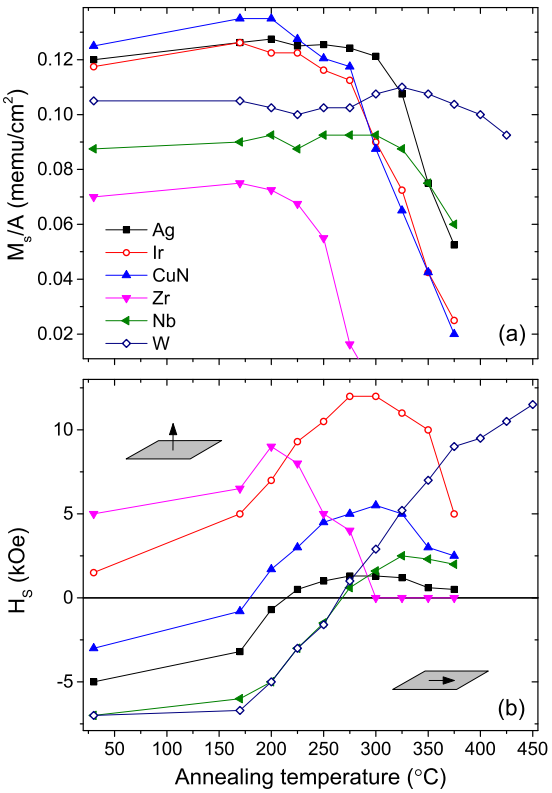

FIG. 2. (Color online) (a) Magnetic moment per unit area and (b) saturation field as a function of the annealing temperature for M/CoFeB/MgO sample with different underlayers.

The highest H_{s} is measured for Ir and CuN buffers, however, they are thermally stable only up to around 300 °C annealing temperature. The transition from the effective in-plane to perpendicular anisotropy for CuN, Ag, and both W and Nb buffers is measured after annealing at 200 °C, 225 °C, and 275 °C, respectively.

In MTJs with an effective PMA of the bottom CoFeB layer we are able to investigate the anisotropy change as a function of the electric field in stack B. We used the method presented in Ref. [18] in order to quantitatively determine the PMA surface energy change for applied bias voltage. We measured the TMR versus the in-plane field curve with the bias voltage applied ranging from $V_{\text{b}} = -1$ V up to 1 V (which correspond to an electric field $E = V/t_{\text{MgO}} = +/- 4$ MV/cm) and from the K_{i} versus the V_{b} slope we obtained the $\Delta K_i/\Delta E$ in units of fJ/Vm. An example of this approach for the sample with the W buffer annealed at 350 °C is presented in Fig. 3. For the estimation of M_{s} we used the moment measured with VSM and a nominal thickness of CoFeB, except from the W buffer case, for which a magnetic dead layer was taken into account (see subsection below). Obtained results are presented in Fig. 4. For all buffer materials except W, both the M_{s}/A and VCMA effects reduce significantly with annealing temperature. In the case of the W buffer, the changes in M_{s}/A and VCMA with annealing temperature are less pronounced. This behavior indicates that perpendicular anisotropy energy and its change with an electric field may be related.

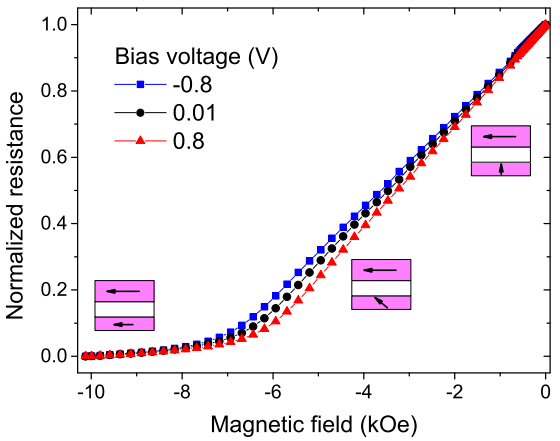

FIG. 3. (Color online) Normalized resistance versus the in-plane magnetic field measured at different bias voltages on the sample with the W buffer annealed at 350 °C. The interface anisotropy energy is calculated for each bias voltage step.

B. W buffer

Now, among the investigated underlayer materials, the biggest VCMA amplitude is measured for the Ir buffer, which is the scope of another publication [15]. However, from the thermal point of view, the most stable system is the one with the W buffer. In contrast to the previously published works with the W seed layer, we observed the transition to PMA, as we used the Fe-rich CoFeB electrode, whereas the Co-rich one was used in Ref. [16] and higher annealing temperature than in Ref. [19]. As a result we obtained a thermally stable trilayer system, with perpendicular magnetic anisotropy and a high tunneling magnetoresistance ratio (TMR). For the annealing temperature of 400 °C the relative difference between resistance at the parallel state and resistance at the zero magnetic field (corresponding to orthogonal alignment between magnetization vectors) reaches 60%, which corresponds to 120% TMR according to the conventional definition. We note that very recently, magnetic and structural studies on PMA in the ferromagnet with the W buffer/capping layer were presented in Ref. [20].

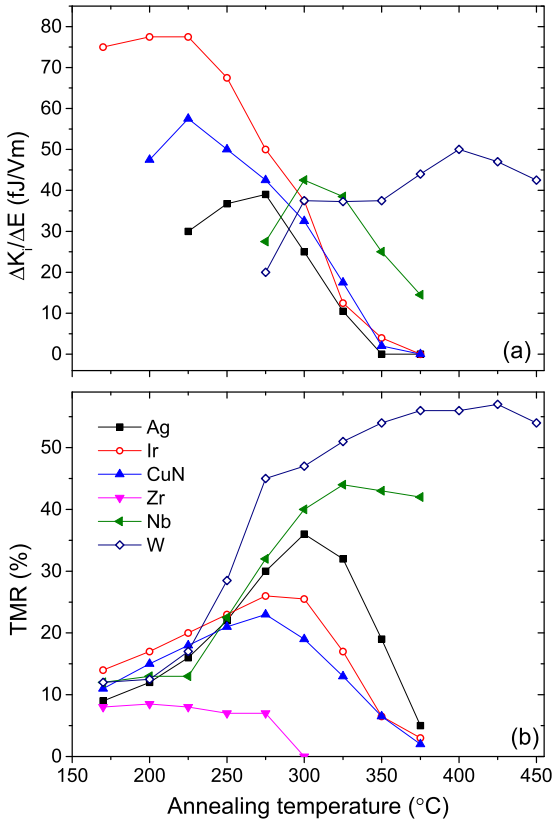

FIG. 4. (Color online) Interface anisotropy energy change per applied electric field (a) and tunneling magnetoresistance (TMR) ratio (b) measured in MTJs with different buffers.

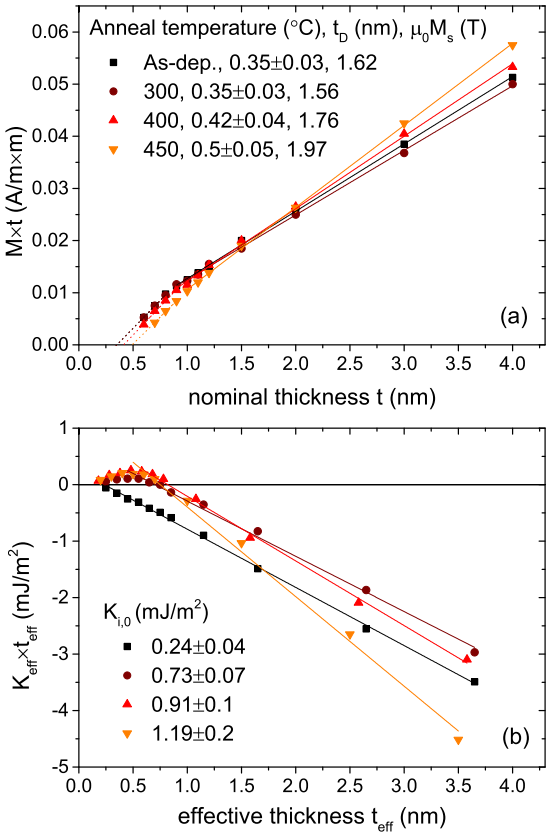

FIG. 5. (Color online) (a) Product of the magnetic moment and CoFeB layer thickness as a function of the nominal thickness t and (b) product of the effective anisotropy and the effective thickness t_{eff} of the bottom CoFeB. Solid lines in (a) represent fits to the thicker CoFeB region, whereas dotted lines are fitted to the thinner CoFeB, for which the magnetic dead layer is determined.

For a precise estimation of the crucial MTJ parameters, such as PMA energy, effective thickness, and saturation magnetization of the CoFeB bottom layer deposited directly onto the W buffer, we have performed VSM measurement of stack A samples with the nominal thickness ranging from 0.6 to 4 nm, in the as-deposited state and after thermal treatment at 300 °C, 400 °C, and 450 °C; see Fig. 5.

In Fig. 5(a) the relation between a product of a magnetic moment and thickness $M \times t$ versus t can be divided into two ranges, for which the dependence is linear with two different slopes. Above the critical thickness of about

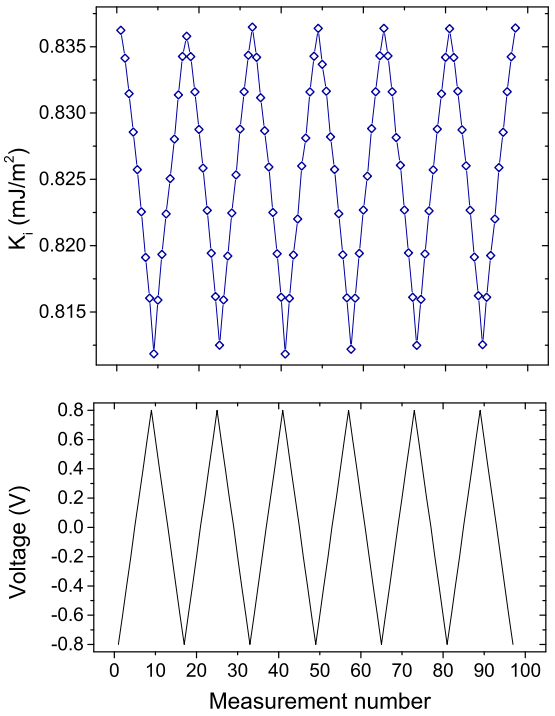

FIG. 6. (Color online) Aging property measured for the MTJ with the W buffer annealed at 350 °C.

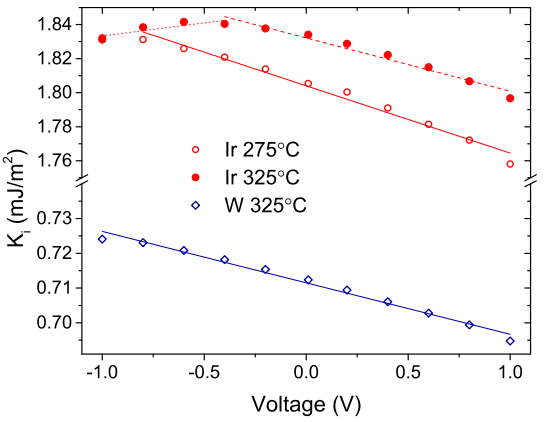

FIG. 7. (Color online) Interface PMA energy dependence on bias voltage after different annealing temperatures. Linear dependence of K_i versus V_b is maintained up to 450 °C in case of the W buffer, whereas for Ir only up to 300 °C.

$t_c = 0.9$ nm the fitting results in the $\mu_0 M_s$ values consistent with the ones expected for the CoFeB alloy. On the other hand, fitting the dependence below t_c gives us the value of magnetic dead layer thickness t_D, however, in this thickness regime the magnetic moment is additionally reduced. This reduction may be explained by incomplete crystallization of CoFeB and coexistence of an amorphous phase [21] or other modification of a film structure [22,23]. In our system we have obtained a magnetic dead layer thickness of 0.35 ± 0.03 nm after the deposition process, which increases to 0.5 ± 0.05 nm after annealing at the highest temperature of 450 °C. The estimated interface anisotropy is already high and equals $K_{i,V=0} = 1.19 \pm 0.2 \mathrm{mJ/m^2}$. Moreover, it is worth noting that by fitting the dependence above the t_c we derived $\mu_0 M_s$ values, which also increase with the annealing temperature. Such behavior is, however, expected, as the B atoms diffuse out from the CoFeB electrode into neighboring layers, which leads to the optimal crystallization after the annealing treatment of 450 °C [24]. We note that for CoFeB thickness of $t = 0.88$ nm, K_{eff} starts to decrease slightly after annealing at 425 °C.

To further elucidate on a thermal stability of the MTJ with the W buffer we have performed aging tests, which were designed as follows. Constant bias voltage was applied and the magnetic anisotropy was derived, which results in a single point in Fig. 6. Then, an interface magnetic anisotropy was calculated for a series of bias voltages scanned back and forth between $V_b = -0.8$ and 0.8 V for a few times. Clearly, properties are not affected by the application of higher bias even after several cycles, which lasted for a few hours.

Finally, we comment on the PMA change induced by electric fields. The measured $\Delta K_i / \Delta E$ values of a few tens of fJ/Vm correspond to previously reported magnitudes [7,8,25,26]. However, we did not observe any sign change between 4d and 5d buffers, as was predicted by Barnes *et al.* in Ref. [12]. We conclude that apart from the buffer materials, the deposition method may play a crucial role in bias voltage effect on PMA, which strongly depends on an interface quality [27].

In the case of the W buffer, the K_i versus V_b dependence is always linear, independent of the annealing temperature. However, in the case of other buffers, like Ir, for example, linear behavior changes into more complicated dependence, after certain annealing steps. Specifically, at negative bias voltage $V_b < -0.5$ V, the positive slope is measured; see Fig. 7. Similar nonlinearity has been measured in the FePd/MgO bilayer [28], which indicates that annealing in the case of MTJs with certain buffers may lead to alloying with the CoFeB electrode. This is further indicated by a sudden drop in the TMR (after annealing) in the case of CuN (275 °C), Ir and Ag (300 °C), and Nb (325 °C).

C. Ferromagnetic resonance

To ensure the potential application in high frequency devices, we investigated the dynamic properties of VCMA using local ferromagnetic resonance (FMR) methods [29]. Figure 8 presents FMR spectra obtained in a sample with the W buffer annealed at 275 °C, which corresponds to the smallest PMA in this case and, thus, the strongest FMR signal. Two peaks were detected at smaller and higher magnetic fields, which are ascribed to the top and bottom CoFeB layers, respectively. Both resonance peaks are asymmetric when no dc bias is applied and change their symmetry with bias. This behavior is attributed to the nonlinear effects induced by the shift in the precession center from the equilibrium point due to the dc voltage-induced torque under the FMR excitation [30,31]. We note that in the case of MTJs with thinner MgO tunnel barriers, the spin-transfer torque effect or dc voltage-dependent reflection coefficient can explain the change in the FMR signal symmetry [32,33]. Moreover, bottom layer FMR frequency depends on the bias voltage. In order to fit the frequency versus the magnetic field dispersion relation we used the macrospin

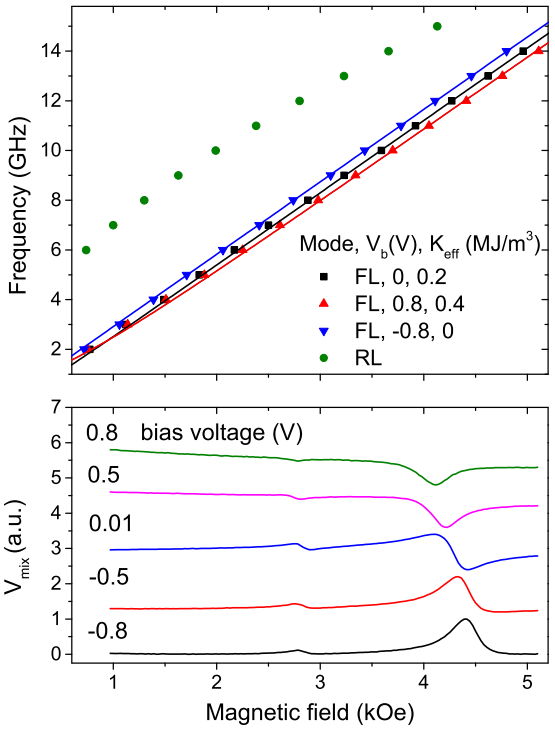

FIG. 8. (Color online) (a) FMR frequency peaks versus the magnetic field applied at 60° from the sample plane for the sample with the W buffer annealed at 275 °C. Lower frequency signal is attributed to the bottom free layer (FL) and its frequency can be further tuned by the application of static bias voltage. Higher frequency signal originates from the top reference layer (RL). (b) FMR spectra obtained at the frequency of $f = 12$ GHz under various bias voltages. Lines are artificially offset for clarity.

model presented elsewhere [15]. For the fitting procedure, the PMA energies were calculated from the VSM measurements. Assuming the change in PMA from $K_{\mathrm{eff}} = 0.2\,\mathrm{mJ/m^3}$ to $K_{\mathrm{eff}} = 0.4\,\mathrm{mJ/m^3}$ for $V_{\mathrm{dc}} = 0.8$ V and to $K_{\mathrm{eff}} = 0$ for $V_{\mathrm{dc}} = -0.8$ V a good agreement with experimentally obtained resonance frequency was obtained; see Fig. 8.

We have confirmed operation in a high frequency regime also after the thermal treatment at higher temperatures, which additionally proves repeatability of electric-field-induced processes and potential high operation speed.

IV. SUMMARY

In summary, we have investigated a seed material influence on PMA and VCMA in *M*/CoFeB/MgO systems. In most of the used buffers we found a decrease in magnetization saturation with annealing temperatures. On the contrary, the in-plane saturating field, which is proportional to PMA energy, increased after annealing up to the point when intermixing between CoFeB and *M* reached a critical value. We speculate that the magnitude of VCMA can be correlated with the in-plane saturation field H_s, i.e., the PMA energy for the annealing temperatures that do not lead to a mixing between the ferromagnet and buffer materials. The trilayer system with the W buffer was found to be thermally stable up to 450 °C, and exhibited transition to PMA after annealing at 275 °C. We measured the change of the anisotropy energy per applied electric field of up to 50 fJ/Vm and the voltage-induced ferromagnetic resonance in this system, which opens new routes for the application of the W material in spintronic devices.

ACKNOWLEDGMENTS

We thank E. Usuda, Y. Sato, S. Tamaru and M. Sekine for assistance with the experiment. This work was funded by the Strategic AIST integrated R&D program, "IMPULSE: Initiative for Most Power-efficient Ultra-Large-Scale data Exploration" and the ImPACT Program of the Council for Science, Technology and Innovation (Cabinet Office, Government of Japan). W.S. acknowledges a Foundation for Polish Science (FNP) scholarship under the START Programme, and AGH University Dean's Grant.

[1] R. L. Stamps, S. Breitkreutz, J. Akerman, A. V. Chumak, Y. Otani, G. E. W. Bauer, J.-U. Thiele, M. Bowen, S. A. Majetich, M. Klui, I. L. Prejbeanu, B. Dieny, N. M. Dempsey, and B. Hillebrands, J. Appl. Phys. D: Applied Physics **47**, 333001 (2014).

[2] M. Weisheit, S. Fahler, A. Marty, Y. Souche, C. Poinsignon, and D. Givord, Science **315**, 349 (2007).

[3] T. Maruyama, Y. Shiota, T. Nozaki, K. Ohta, N. Toda, M. Mizuguchi, A. A. Tulapurkar, T. Shinjo, M. Shiraishi, S. Mizukami, Y. Ando, and Y. Suzuki, Nature Nanotechnology **4**, 158 (2009).

[4] T. Nozaki, Y. Shiota, M. Shiraishi, T. Shinjo, and Y. Suzuki, Appl. Phys. Lett. **96**, 022506 (2010).

[5] Y. Shiota, T. Nozaki, F. Bonell, S. Murakami, T. Shinjo, and Y. Suzuki, Nature Materials **11**, 39 (2012).

[6] W.-G. Wang, M. Li, S. Hageman, and C. L. Chien, Nature Materials **11**, 64 (2012).

[7] L. Liu, C.-F. Pai, D. Ralph, and R. Buhrman, Phys. Rev. Lett. **109**, 186602 (2012).

[8] W. Skowroński, P. Wiśniowski, T. Stobiecki, S. Cardoso, P. P. Freitas, and S. v. Dijken, Appl. Phys. Lett. **101**, 192401 (2012).

[9] A. Schellekens, A. van den Brink, J. Franken, H. Swagten, and B. Koopmans, Nature Communications **3**, 847 (2012).

[10] D. Chiba, S. Fukami, K. Shimamura, N. Ishiwata, K. Kobayashi, and T. Ono, Nature Materials **10**, 853 (2011).

[11] T. Nozaki, K. Yakushiji, S. Tamaru, M. Sekine, R. Matsumoto, M. Konoto, H. Kubota, A. Fukushima, and S. Yuasa, Appl. Phys. Express **6**, 073005 (2013).

[12] S. E. Barnes, J. Ieda, and S. Maekawa, Scientific Reports **4**, (2014).

[13] Y. Shiota, F. Bonell, S. Miwa, N. Mizuochi, T. Shinjo, and Y. Suzuki, Appl. Phys. Lett. **103**, 082410 (2013).

[14] A. A. Tulapurkar, Y. Suzuki, A. Fukushima, H. Kubota, H. Maehara, K. Tsunekawa, D. D. Djayaprawira, N. Watanabe, and S. Yuasa, Nature (London) **438**, 339 (2005).

[15] W. Skowroński, T. Nozaki, Y. Shiota, S. Tamaru, K. Yakushiji, H. Kubota, A. Fukushima, S. Yuasa, and Y. Suzuki, Appl. Phys. Express **8**, 053003 (2015).

[16] D. C. Worledge, G. Hu, D. W. Abraham, P. L. Trouilloud, and S. Brown, J. Appl. Phys. **115**, 172601 (2014).
[17] J. Y. Bae, W. C. Lim, H. J. Kim, T. D. Lee, K. W. Kim, and T. W. Kim, J. Appl. Phys. **99**, 08T316 (2006).
[18] Y. Shiota, S. Murakami, F. Bonell, T. Nozaki, T. Shinjo, and Y. Suzuki, Appl. Phys. Express **4**, 043005 (2011).
[19] C.-F. Pai, M.-H. Nguyen, C. Belvin, L. H. Vilela-Leo, D. C. Ralph, and R. A. Buhrman, Appl. Phys. Lett. **104**, 082407 (2014).
[20] G.-G. An, J.-B. Lee, S.-M. Yang, J.-H. Kim, W.-S. Chung, and J.-P. Hong, Acta Materialia **87**, 259 (2015).
[21] J. Sinha, M. Hayashi, A. J. Kellock, S. Fukami, M. Yamanouchi, H. Sato, S. Ikeda, S. Mitani, S.-h. Yang, S. S. P. Parkin, and H. Ohno, Appl. Phys. Lett. **102**, 242405 (2013).
[22] N. Miyakawa, D. C. Worledge, and K. Kita, IEEE Magn. Lett. **4**, 1000104 (2013).
[23] C. C. Tsai, C.-W. Cheng, M.-C. Tsai, and G. Chern, IEEE Trans. Magn. **50**, 1401404 (2014).
[24] S. Ikeda, J. Hayakawa, Y. Ashizawa, Y. M. Lee, K. Miura, H. Hasegawa, M. Tsunoda, F. Matsukura, and H. Ohno, Appl. Phys. Lett. **93**, 082508 (2008).
[25] M. Endo, S. Kanai, S. Ikeda, F. Matsukura, and H. Ohno, Appl. Phys. Lett. **96**, 212503 (2010).
[26] V. B. Naik, H. Meng, J. X. Xiao, R. S. Liu, A. Kumar, K. Y. Zeng, P. Luo, and S. Yap, Appl. Phys. Lett. **105**, 052403 (2014).
[27] T. Koyama, A. Obinata, Y. Hibino, and D. Chiba, Appl. Phys. Express **6**, 123001 (2013).
[28] F. Bonell, S. Murakami, Y. Shiota, T. Nozaki, T. Shinjo, and Y. Suzuki, Appl. Phys. Lett. **98**, 232510 (2011).
[29] T. Nozaki, Y. Shiota, S. Miwa, S. Murakami, F. Bonell, S. Ishibashi, H. Kubota, K. Yakushiji, T. Saruya, A. Fukushima, S. Yuasa, T. Shinjo, and Y. Suzuki, Nature Physics **8**, 492 (2012).
[30] Y. Shiota, S. Miwa, S. Tamaru, T. Nozaki, H. Kubota, A. Fukushima, Y. Suzuki, and S. Yuasa, Appl. Phys. Lett. **105**, 192408 (2014).
[31] S. Miwa, S. Ishibashi, H. Tomita, T. Nozaki, E. Tamura, K. Ando, N. Mizuochi, T. Saruya, H. Kubota, and K. Yakushiji, Nature Materials **13**, 50 (2014).
[32] W. Skowroński, M. Frankowski, J. Wrona, T. Stobiecki, P. Ogrodnik, and J. Barnaś, Appl. Phys. Lett. **105**, 072409 (2014).
[33] S. Kanai, M. Gajek, D. C. Worledge, F. Matsukura, and H. Ohno, Appl. Phys. Lett. **105**, 242409 (2014).